JOURNAL OF COMPUTATIONAL PHYSICS 12, 435–461 (1973)

The Method of the False Transient for the Solution of Coupled Elliptic Equations

G. D. MALLINSON AND G. DE VAHL DAVIS

School of Mechanical and Industrial Engineering,
University of New South Wales, Kensington, Australia 2033

Received July 11, 1972

A method for the numerical solution of a system of coupled, nonlinear elliptic partial differential equations is described, and the application of the method to the equations governing steady, laminar natural convection is presented. The essential feature of the method is the conversion of the equations to a parabolic form by the addition of false time derivatives, thus, enabling a marching solution, equivalent to a single iterative procedure, to be used. The method is evaluated by applying it to a well known two-dimensional problem and some examples of its use in three dimensions are given.

1. INTRODUCTION

The work described herein was developed during a study of the buoyancy-driven motion of a viscous incompressible fluid in an enclosure. Typical of such problems are the transfer of heat across the cavity of a double-glazed window and the cooling of a turbine blade using a closed thermosyphon. In many such practical applications, the motion is steady and laminar, and the resultant governing equations are elliptic. Numerical procedures must be employed for their solution. In general, the motion is also three-dimensional, but because the numerical procedures involve a double iteration scheme which is lengthy and expensive, it has almost invariably been assumed that a two-dimensional model is adequate. In order to explore the validity of this assumption, an efficient solution procedure for three-dimensional problems was sought.

There are two approaches which may be adopted. We may solve the set of equations written in what are called the primitive variables, viz., velocity components and pressure. Typical of this approach is the work of Williams [1] and Chorin [2]. Alternatively, the equations may be formulated in terms of vorticity and a vector potential. The only solutions obtained in this way that we have seen are those of Aziz and Hellums [3] and Holst and Aziz [4], although the corresponding two-dimensional formulation (in terms of vorticity and stream function) has

been widely used by, for example, Torrance [5], Wilkes and Churchill [6] and de Vahl Davis [7]. In two dimensions, this approach is attractive because, first, it reduces the number of equations to be solved from four to three, and, second, it ensures that the continuity equation is automatically satisfied; as discussed by Piacsek and Williams [8], failure to satisfy continuity using the primitive variable equations can lead to convective instability. Moreover, the difficulties associated with pressure boundary conditions are avoided, the corresponding conditions for vorticity being much simpler and more easily applied. Finally, Aziz and Hellums [3] found that the iterative procedure based on the primitive variable equations was less satisfactory in its convergence behavior.

In either approach, the steady solution may be found by directly solving the steady equations, or by solving the unsteady equations, all but one of which become parabolic. We may then proceed through time until the solution ceases to change significantly. When the steady equations are solved, a double iterative scheme is necessary since they are elliptic and coupled. When the unsteady equations are solved, the outer iteration is replaced by a progression through time. Although the number of equations involved in the inner iteration is now less, the corrective procedures necessary to ensure that the transient is faithfully followed (e.g., Pearson [9] and Thomas and de Vahl Davis [10]) still cause the solution process to be lengthy.

In very many situations, however, we are interested only in the final steady state, and all of the foregoing procedures are, therefore, inefficient. If the steady solution exists and is unique, it may be obtained more efficiently by the introduction into the governing equations of false transient terms.

This is the basis of the method we propose here. The false transient terms lead to a set of parabolic equations which are solved by marching through a distorted time; no inner iterations are involved and the rate of transient convergence can be enhanced by the use of different time steps for the different equations. The true transient solution is lost, but at large times the transient terms decay and the true steady solution is recovered.

We have applied the method to a number of natural convection problems. For a two-dimensional situation, extensive tests on the accuracy and speed of the method have been performed. It was found that the method was at least one and perhaps two orders of magnitude faster than a conventional, double iterative procedure. We have also solved a number of three-dimensional problems, obtaining solutions typically in about 100 "time" steps, the total computer time being of the order of ten minutes on an IBM 360/50 for 1331 mesh points. Finer meshes have been used; the solution time varying roughly in proportion to the number of mesh points.

In the next section, the Navier–Stokes and energy equations for three-dimensional flow of a viscous incompressible fluid are transformed into equations for vorticity

and vector potential. The boundary conditions are discussed, and the false transient terms introduced. In Section 3, the finite difference equations and the alternating direction implicit method used for their solution are described. The reduction to two dimensions follows in Section 4. In Section 5 a comparison is made between the method of the false transient and the method applied by Rubel and Landis [11] to a two-dimensional natural convection problem. Some results for three-dimensional problems are given in Section 6, although a detailed discussion is beyond the scope of this paper, the principal purpose of which is to describe the solution procedure.

2. The False Transient Equations

It is common in studies of natural convection to make the Boussinesq [12] approximation, i.e., to assume that the effect of temperature on density is confined to the body force term of the momentum equation and that otherwise the thermodynamic and transport properties of the fluid are independent of temperature and pressure. This implies that the fluid is essentially incompressible, and that its equation of state is

$$\rho = \rho_0(1 - \beta[T - T_0]),$$

where ρ, β and T denote respectively the density, volumetric expansion coefficient, and temperature of the fluid, and the subscript denotes some reference state. Further, making the reasonable assumption that viscous dissipation is negligible, the equations of motion and energy may be written

$$\frac{D\bar{u}}{Dt} = -\nabla p/\rho_0 - \beta(T - T_0)\,\bar{g} + \nu\nabla^2\bar{u}, \tag{1}$$

$$\nabla \cdot \bar{u} = 0, \tag{2}$$

$$\frac{DT}{Dt} = \kappa\nabla^2 T, \tag{3}$$

where $\bar{u}$ is the velocity vector, p is the perturbation of static pressure from the first order hydrostatic value ($\rho_0 gz$), ν and κ are the kinematic viscosity and thermal diffusivity, respectively, $\bar{g}$ is the gravitational vector, and t is time. Using the vector identity,

$$(\nabla \times \bar{u}) \times \bar{u} = \bar{u} \cdot \nabla\bar{u} - \nabla\bar{u}^2/2,$$

together with the continuity equation (2), Eqs. (1) and (3) may be written

$$\frac{\partial \bar{u}}{\partial t} = -(\nabla \times \bar{u}) \times \bar{u} - \nabla P/\rho_0 - \beta(T - T_0)\,\bar{g} + \nu\nabla^2\bar{u}, \tag{4}$$

$$\frac{\partial T}{\partial t} = -\nabla \cdot (\bar{u}T) + \kappa\nabla^2 T, \tag{5}$$

where P denotes the total pressure $p + \rho_0\bar{u}^2/2$.

Using L (a dimension of the cavity), L^2/κ, κ/L, and $\rho_0\kappa^2/L^2$ as scale factors for length, time, velocity, and pressure, respectively, and introducing $\theta = (T - T_0)/(T_1 - T_0)$, where T_0 and T_1 are fixed reference temperatures, Eqs. (4) and (5) become

$$\frac{\partial \bar{u}}{\partial t} = -(\nabla \times \bar{u}) \times \bar{u} - \nabla P - \mathrm{RaPr}\,\theta\hat{\bar{g}} + \mathrm{Pr}\,\nabla^2\bar{u}, \tag{6}$$

$$\frac{\partial \theta}{\partial t} = -\nabla \cdot (\bar{u}\theta) + \nabla^2\theta, \tag{7}$$

where all the variables have been made nondimensional, and where $\mathrm{Ra} = g\beta(T_1 - T_0)L^3/\kappa\nu$ is the Rayleigh number and $\mathrm{Pr} = \nu/\kappa$ is the Prandtl number.

Since $\bar{u}$ is soleniodal, it can be expressed in the Eulerian form [13]

$$\bar{u} = \nabla f \times \nabla g,$$

where the surfaces,

$$f = c_1\,, \tag{9}$$

$$g = c_2\,, \tag{10}$$

are vector sheets of $\bar{u}$. (Although the functions f and g would permit a useful geometric interpretation to be made, their direct use would necessitate the numerical solution of highly nonlinear equations, which is computationally difficult.) We may now add the term $\nabla \times \nabla h$ (which is identically zero) to the right side of (8) which, upon rearrangement, leads to

$$\bar{u} = \nabla \times (f\nabla g + \nabla h) = \nabla \times \bar{\Psi}, \qquad \text{say.}$$

It is always possible to choose h such that $\nabla \cdot \bar{\Psi}$ vanishes. In such a case, $\bar{\Psi}$ is a solenoidal vector potential for $\bar{u}$.

Since vorticity is the curl of the velocity vector, it follows that

$$\bar{\zeta} = \nabla \times \bar{u} = \nabla \times \nabla \times \bar{\Psi} = \nabla(\nabla \cdot \bar{\Psi}) - \nabla^2\bar{\Psi}$$
$$= -\nabla^2\bar{\Psi},$$

since $\bar{\Psi}$ is solenoidal. Equations (2) and (4) may now be replaced by the set

$$\frac{\partial \bar{\zeta}}{\partial t} = -\nabla \times (\bar{\zeta} \times \bar{u}) - \mathrm{RaPr}(\nabla \times \theta \hat{\bar{g}}) + \mathrm{Pr}\, \nabla^2 \bar{\zeta}, \tag{11}$$

$$0 = \nabla^2 \bar{\Psi} + \bar{\zeta}, \tag{12}$$

$$\bar{u} = \nabla \times \bar{\Psi}. \tag{13}$$

Equations (11)–(13), together with (7), are to be solved for the velocity and temperature fields.

The method of the false transient makes two simple changes to this set of equations: a fictitious transient term is inserted on the left side of (12), and the time derivatives in (11) and (12) are given modified coefficients. The equation set then becomes

$$\frac{\mathrm{Pr}}{\alpha_\zeta} \frac{\partial \bar{\zeta}}{\partial t} = -\nabla \times (\bar{\zeta} \times \bar{u}) - \mathrm{RaPr}(\nabla \times \theta \hat{\bar{g}}) + \mathrm{Pr}\, \nabla^2 \bar{\zeta}, \tag{14}$$

$$\frac{1}{\alpha_\psi} \frac{\partial \bar{\Psi}}{\partial t} = \nabla^2 \bar{\Psi} + \bar{\zeta}, \tag{15}$$

$$\frac{\partial \theta}{\partial t} = -\nabla \cdot (\bar{u}\theta) + \nabla^2 \theta. \tag{7}$$

If a steady state exists, clearly it will be reached using either set of equations.

The method is a generalization of the device mentioned by Dorodnicyn [14] and employed in the artificial compressibility technique of Chorin [15]. In contrast with the latter, however, this method uses a purely artificial construction and could be applied to any set of elliptic equations. The reasons for these changes will be discussed in Section 3.2.

We now turn to consider the boundary conditions for these equations, which are to be solved in the three-dimensional region bounded by the planes $x = 0, 1$, $y = 0, Y$, $z = 0, Z$, as illustrated in Fig. 1.

The specification of boundary conditions for the vector potential has been fully discussed by Hirasaki and Hellums [16]. For a plane, impermeable surface, the vector is normal to the surface and its gradient is zero. For the surface $x = 0$, for example,

$$(\partial \psi_1 / \partial x) = 0, \qquad \psi_2 = \psi_3 = 0,$$

where $\bar{\Psi} = \psi_1 i + \psi_2 j + \psi_3 k$. At nonslip surfaces, the tangential derivatives of the velocity components are zero. Thus, at $x = 0$, the vorticity components become

$$\zeta_1 = 0, \qquad \zeta_2 = -\partial w / \partial x, \qquad \zeta_3 = \partial v / \partial x,$$

where $\bar{\zeta} = \zeta_1 i + \zeta_2 j + \zeta_3 k$, and $\bar{u} = ui + vj + wk$.

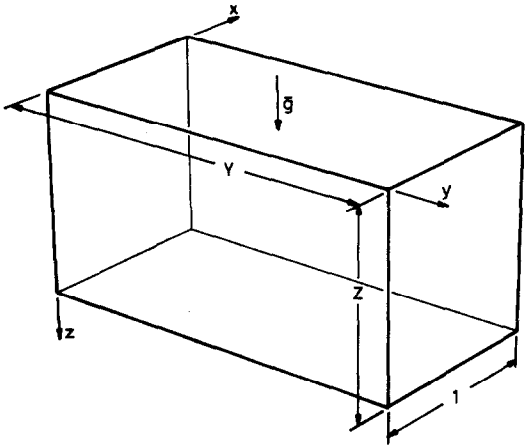

FIG. 1. The solution region and coordinate orientation. Thermal boundary conditions are: at $x = 0, 1$: $\theta = x$; at $y = 0$, Y: $\partial\theta/\partial y = 0$; at $z = 0$, Z: $\partial\theta/\partial z = 0$. All surfaces are stationary, impermeable, and nonslip.

Aziz and Hellums [3] used these boundary conditions. However, there is a difficulty associated with their use. For if the velocity derivatives are approximated using two-point forward differences, the accuracy is only of order Δx; if three-point forward formulas are used, a very fine mesh would be required if a boundary layer exists; and finally, if three-point central differences are used, the boundary conditions on the tangential velocity components do not appear explicitly in the difference approximations. Since this is, of course, desirable, the following alternative formulation has been used. Because

$$w = \partial\psi_2/\partial x - \partial\psi_1/\partial y, \tag{16}$$

the condition on ζ_2 at $x = 0$ becomes

$$\zeta_2 = -\partial^2\psi_2/\partial x^2 + \partial^2\psi_1/\partial x\partial y.$$

Assuming ψ_1 to be sufficiently smooth,

$$\zeta_2 = -\partial^2\psi_2/\partial x^2 + \partial^2\psi_1/\partial y\partial x = -\partial^2\psi_2/\partial x^2, \tag{17}$$

and since

$$\begin{aligned} v &= \partial\psi_1/\partial z - \partial\psi_3/\partial x, \\ \zeta_3 &= -\partial^2\psi_3/\partial x^2. \end{aligned} \tag{18}$$

In the application of these conditions to the finite difference approximations, as

discussed in the next section, the integrals of ζ_2 and ζ_3 are required; values of $\partial\psi_2/\partial x$ and $\partial\psi_3/\partial x$ at the boundary are, therefore, needed. From (16),

$$\partial\psi_2/\partial x = \partial\psi_1/\partial y + w,$$

and similarly

$$\partial\psi_3/\partial x = \partial\psi_1/\partial z - v.$$

For stationary walls, $v = w = 0$ and, therefore,

$$\frac{\partial\psi_2}{\partial x}\Big|_{x=0} = \frac{\partial\psi_1}{\partial y}\Big|_{x=0} \quad \text{and} \quad \frac{\partial\psi_3}{\partial x}\Big|_{x=0} = \frac{\partial\psi_1}{\partial z}\Big|_{x=0}.$$

The complete set of boundary conditions on Ψ and ζ are shown in Table I.

The conditions on θ are, in comparison, quite simple. We may specify the temperature or the heat flux at a surface, thereby imposing a condition on θ or its normal derivative. In the problems described later, we will specify differing uniform temperatures on two opposite vertical surfaces and require the remaining surfaces to be adiabatic.

3. Numerical Solution of the Equations

Equations (7), (14), and (15) must be solved numerically. If we seek to solve the steady equations, in which the left sides are all zero, a double iterative procedure is necessary. Typically, distributions of Ψ, ζ, and θ are assumed. The linearizing assumption that these equations may be regarded as equations solely for Ψ, ζ, and θ respectively, is made. The finite difference approximations to the component equations are then solved iteratively until convergence is obtained. However, because the equations are elliptic, the solution of each is an iterative process and the solution procedure is, therefore, very lengthy.

The true transient equations can be solved rather more rapidly because (7) and (11), being parabolic, can be advanced through one time step by a direct, rather than an iterative, procedure.

The essential feature of our method is the conversion of all equations to parabolic form, by the insertion of the false transient term into (12). Each equation may be advanced through time by a direct method and the complete solution procedure may be regarded as a single iterative scheme.

3.1. *Finite Difference Approximations*

The method will be illustrated by considering the finite difference approximation to the equation for the x-component of vorticity. The full set of differential and difference equations appears in Appendix A.

The equation for ζ_1 is

$$\frac{\mathrm{Pr}}{\alpha_\zeta}\frac{\partial \zeta_1}{\partial t} = -\frac{\partial}{\partial y}(\zeta_1 v) - \frac{\partial}{\partial z}(\zeta_1 w) + \frac{\partial}{\partial y}(\zeta_2 u) + \frac{\partial}{\partial z}(\zeta_3 u) - \mathrm{RaPr}\frac{\partial \theta}{\partial y} + \mathrm{Pr}\left\{\frac{\partial^2 \zeta_1}{\partial x^2} + \frac{\partial^2 \zeta_1}{\partial y^2} + \frac{\partial^2 \zeta_1}{\partial z^2}\right\}. \tag{19}$$

It will be noted that the equation is written in conservative form, i.e., in a form which guarantees conservation of vorticity both in the differential equation and in the difference approximation and, moreover, results in a somewhat simplified expression for convection (in comparison with that used by Aziz and Hellums [3]).

A uniform mesh is used. Mesh point variables are typically denoted by $\zeta_1(i, j, k)$; however, the notation is rendered more compact by omitting arguments when they have the default values i, j or k. Thus, $\zeta_1(i-1)$ denotes $\zeta_1(i-1, j, k)$. Central differences are used throughout, the notation being

$$\delta_x \zeta_1 = (\zeta_1(i+1) - \zeta_1(i-1))/2\Delta x$$

and

$$\delta_x{}^2 \zeta_1 = (\zeta_1(i+1) - 2\zeta_1 + \zeta_1(i-1))/\Delta x^2.$$

The finite difference approximation to (19) may now be written

$$\frac{\mathrm{Pr}}{\alpha_\zeta}\frac{\partial \zeta_1}{\partial t} = -\delta_y(\zeta_1 v) - \delta_z(\zeta_1 w) + \delta_y(\zeta_2 u) + \delta_z(\zeta_3 u) - \mathrm{RaPr}\,\delta_y\theta + \mathrm{Pr}(\delta_x{}^2\zeta_1 + \delta_y{}^2\zeta_1 + \delta_z{}^2\zeta_1), \tag{20}$$

where the transient term has not yet been discretized. In expanded form this becomes

$$\begin{aligned}\frac{\mathrm{Pr}}{\alpha_\zeta}\frac{\partial \zeta_1}{\partial t} = {} & -(v(j+1)\,\zeta_1(j+1) - v(j-1)\,\zeta_1(j-1))/2\,\Delta y \\ & - (w(k+1)\,\zeta_1(k+1) - w(k-1)\,\zeta_1(k-1))/2\,\Delta z \\ & + (u(j+1)\,\zeta_2(j+1) - u(j-1)\,\zeta_2(j-1))/2\,\Delta y \\ & + (u(k+1)\,\zeta_3(k+1) - u(k-1)\,\zeta_3(k-1))/2\,\Delta z \\ & - \mathrm{RaPr}(\theta(j+1) - \theta(j-1))/2\,\Delta y \\ & + \mathrm{Pr}((\zeta_1(i+1) - 2\zeta_1 + \zeta_1(i-1))/\Delta x^2 \\ & + (\zeta_1(j+1) - 2\zeta_1 + \zeta_1(j-1))/\Delta y^2 \\ & + (\zeta_1(k+1) - 2\zeta_1 + \zeta\,(k-1))/\Delta z^2).\end{aligned}$$

Boundary conditions on Ψ and θ are applied in the usual manner, using central differences and image points for derivative conditions. Vorticity boundary conditions are obtained using the technique introduced by Gosman *et al.*, [17]. It is assumed that, in the vicinity of a wall, vorticity varies linearly with wall distance, i.e., that

$$\zeta_2 = \zeta_2(1, j, k) + (\zeta_2(2, j, k) - \zeta_2(1, j, k))x/\Delta x, \tag{21}$$

for ζ_2 near $x = 0$. Upon insertion of (21) into (17), the latter may be integrated over the first mesh interval to yield

$$\zeta_2(1, j, k) = 3\left(-\psi_2(2, j, k) + \Delta x \left.\frac{\partial \psi_2}{\partial x}\right|_{x=0}\right)\Big/\Delta x^2 - \zeta_2(2, j, k)/2. \tag{22}$$

A central difference approximation is used to evaluate $(\partial\psi_2/\partial x)_{x=0}$, viz.

$$\begin{aligned}(\partial\psi_2/\partial x)_{x=0} &= (\partial\psi_1/\partial y)_{x=0} \\ &\simeq (\psi_1(1, j+1) - \psi_1(1, j-1))/(2\Delta y).\end{aligned}$$

3.2. *Solution Procedure*

Equation (20) can be written

$$\frac{\Pr}{\alpha_\zeta}\frac{\partial \zeta_1}{\partial t} = (a_x + a_y + a_z)\,\zeta_1 + s(u, \zeta_2, \zeta_3, \theta),$$

where a_x, a_y, a_z, and s are point operators defined as follows:

$$\begin{aligned}a_x\zeta_1 &= \Pr\,\delta_x{}^2\zeta_1, \\ a_y\zeta_1 &= \Pr\,\delta_y{}^2\zeta_1 - \delta_y(v\zeta_1), \\ a_z\zeta_1 &= \Pr\,\delta_z{}^2\zeta_1 - \delta_z(w\zeta_1), \\ s(u, \zeta_2, \zeta_3, \theta) &= \delta_y(u\zeta_2) + \delta_z(u\zeta_3) - \mathrm{RaPr}\,\delta_y\theta.\end{aligned}$$

The set of point equations can then be written in matrix form as

$$\frac{\Pr}{\alpha_\zeta}\frac{\partial}{\partial t}[\zeta_1] = (A_x + A_y + A_z)[\zeta_1] + [s],$$

where quantities in square brackets are column vectors and A_x, A_y, and A_z are matrices.

An equation of this form may be advanced through time using an alternating direction implicit procedure. The one we have used is a variation described by

Samarskii and Andreev [18] of the scheme proposed independently by Douglas [19] and Brian [20]. The equations to advance ζ_1^n to ζ_1^{n+1} are

$$
\begin{aligned}
(I - rA_x)[\omega^*] &= (A_x + A_y + A_z)[\zeta_1^n] + [s(u^n, \zeta_2^n, \zeta_3^n, \theta^n)], \\
(I - rA_y)[\omega^{**}] &= [\omega^*], \\
(I - rA_z)[\omega^{***}] &= [\omega^{**}], \\
[\zeta_1^{n+1}] &= [\zeta_1^n] + 2r[\omega^{***}],
\end{aligned}
$$

where $r = \Delta t \alpha_\zeta / 2\mathrm{Pr}$ and Δt denotes the time increment; the ω's are intermediate variables. The coefficient α_ζ is used to enhance transient convergence as discussed more fully later.

This method was chosen for its efficiency in terms of the number of operations required per time step. Although Chorin [2] used an even simpler scheme (reported in an earlier paper [21] of Samarskii), that scheme is not satisfactory because it contains a truncation error of order Δt which does not decay with time. The correct solution of the finite difference approximations of the steady equations cannot, therefore, be obtained unless prohibitively small time steps are employed.

It can be shown that, for a single linear equation, the Samarskii–Andreev method is unconditionally stable. We have performed a test calculation (on a linear diffusion equation) in which solutions were obtained using time steps as large as $160\,\Delta x^2$. The number of time steps to convergence rose drastically, but the correct steady solution was eventually reached. It is, unforunately, not possible to prove (or disprove) the stability of the scheme when applied to coupled, nonlinear equations. Our experience has shown that, with suitable choices for the parameters α_ζ and α_ψ, this method is superior to that of Peaceman–Rachford [22] for two-dimensional problems. Thomas and de Vahl Davis [10], by computing the spectral radius of the amplification matrix for each equation, showed that the latter is stable for all Δt when applied to a nonlinear (natural convection) problem. We, therefore, conclude that the Samarskii–Andreev method is stable for a single equation. However, instability can still be introduced by the coupling between equations of a system. There are two grounds for this belief. First, we have observed that despite the foregoing, there is an upper limit on the usable time step when solving a system (in contrast to the case of a single equation). It is $0.8\,\Delta x^2$ when $\alpha_\zeta = \alpha_\psi = 1$, in either two or three dimensions. For any values of Ra and Pr, solutions can be obtained if Δt is chosen to satisfy this condition. Second, if this condition is violated, the instability can still be controlled if either α_ζ or α_ψ is reduced; that is, the effective Δt for one of the equations can be increased above this limit, if that for another equation is reduced. This suggests that the oscillations which would otherwise develop must be due to an interaction between the equations.

The insertion of Pr on the left side of (14) had the effect of adjusting the development of the vorticity transient in cases where $\mathrm{Pr} \neq 1$. It was found that this device made the total solution time more or less independent of Pr.

3.3. *Overall Solution Procedure*

The general arrangement of the solution procedure is quite simple. The main iterative loop starts with the advancement through one time step of $\bar{\Psi}$ using Eq. (15). The three components ψ_1, ψ_2, and ψ_3 are found in turn. This is followed by calculation of new velocity fields (Eq. (13)) and vorticity boundary conditions. A new θ field is then found (Eq. (7)). Finally, new values for ζ_1, ζ_2, and ζ_3 are obtained from Eq. (14).

To start the procedure, distributions of $\bar{\Psi}$ and θ are set, and corresponding values for $\bar{\zeta}$ and $\bar{u}$ are computed for the finite difference approximations to (12) and (13) and the appropriate boundary conditions. The main loop is entered at the point where Eq. (7) is used to update the temperature field.

The cycle is continued until convergence is reached. The sum of the absolute values of the changes from one iteration to the next of all mesh point values of the three components of $\bar{\Psi}$ is calculated; the corresponding quantities for $\bar{\zeta}$ and θ are also found. These three numbers are then normalized using selected values of the respective quantities. Strictly speaking, we should perhaps seek the maximum value at each iteration. However, this seems unnecessary; instead, values are selected which are known to be at or near the maxima. Convergence is declared to have been reached when the three normalized numbers are less than some specified small value—typically 10^{-5}—for two successive iterations (the last requirement being intended to prevent premature termination of the iterations at the turning point of a slowly oscillatory solution). Further checks on convergence include an examination of plots of transient values of selected mesh point variables.

It should, perhaps, be mentioned that the vector potential-vorticity formulation for three-dimensional problems requires a large storage capacity. We carry 13 fields—ζ_1, ζ_2, ζ_3, ψ_1, ψ_2, ψ_3, θ, u, v, w, and three work spaces—for the A.D.I. solution algorithm (the three components of vorticity are advanced simultaneously). This could be reduced to eight by computing the velocities when needed and by solving for the three components of vorticity consecutively; however, an increase in solution time would be incurred. These figures are to be compared with a minimum of six fields if the primitive variables are used (u, v, w, p, θ, and one work space). Thus, for an 11 by 11 by 11 mesh, 17, 303 words are required for main data storage, and the total program size is approximately 32,000 words. Using an IBM 360/50 computer with a million bytes of core a complete iteration cycle for an 11 by 11 by 11 field requires about 5 sec.

4. Equations for Two-Dimensional Flow

It would be useful if we could assess the speed and accuracy of the present method by a comparison of results with those previously obtained for three-dimensional flows. However, this is not possible. Chorin [2] did not carry his solution to steady state, commenting that this would have been excessively time consuming on the computer; 430 time steps were completed, but virtually no quantitative information is presented for the final state. Williams [1] used cylindrical polar coordinates, and we have so far only programmed the rectangular Cartesian case. We are doubtful of the validity of the results of Aziz and Hellums [3], for reasons which will be discussed in Section 6. In any event, a meaningful speed comparison can not be made since their solution was obtained on an IBM 7040 computer, to which we did not have access. They required about four minutes per iteration on that machine. Finally, Holst and Aziz [4] solved the problem of natural convection in a porous medium, for which the equations are somewhat simpler.

Accordingly, tests were conducted on related two-dimensional problems. Of course, accuracy is a feature of the spatial finite difference approximations, rather than of the technique used to find the steady solution. Since we have ensured that the transient terms decay to zero, it would be expected that quadratic convergence would be achieved by the use of central spatial differences and that the false transient method would have no effect on this. Convergence was investigated during a study of false diffusion in numerical fluid dynamics. The results have been reported elsewhere [23], although the method was not described. It was found that quadratic convergence is achieved provided that the nonlinear terms do not cause a thin boundary layer to form; in such cases, convergence becomes approximately linear and a nonuniform mesh is recommended.

We are principally concerned here with the transient behavior of the method, and to examine this we used the problem of natural convection in a rectangular enclosure heated from the side. The governing equations for this problem may be obtained directly from the three-dimensional equations presented before. Setting v and all y-derivatives to zero, these become

$$\frac{\mathrm{Pr}}{\alpha_\zeta}\frac{\partial \zeta_2}{\partial t} = -\frac{\partial}{\partial x}(u\zeta_2) - \frac{\partial}{\partial z}(w\zeta_2) + \mathrm{RaPr}\frac{\partial \theta}{\partial x} + \mathrm{Pr}\left(\frac{\partial^2 \zeta_2}{\partial x^2} + \frac{\partial^2 \zeta_2}{\partial z^2}\right), \tag{23}$$

$$\frac{1}{\alpha_\psi}\frac{\partial \psi_2}{\partial t} = \frac{\partial^2 \psi_2}{\partial x^2} + \frac{\partial^2 \psi_2}{\partial z^2} + \zeta_2, \tag{24}$$

$$\frac{\partial \theta}{\partial t} = -\frac{\partial (u\theta)}{\partial x} - \frac{\partial (w\theta)}{\partial z} + \frac{\partial^2 \theta}{\partial x^2} + \frac{\partial^2 \theta}{\partial z^2}, \tag{25}$$

$$u = -\frac{\partial \psi_2}{\partial z}, \tag{26}$$

$$w = \frac{\partial \psi_2}{\partial x}. \tag{27}$$

The boundary conditions are obtained in a similar manner from those presented in Table I. It may be noted that ψ_2, the only nonvanishing component of the vector potential, becomes the familiar two-dimensional stream function.

TABLE I

Boundary Conditions for Ψ and ξ at Impermeable Nonslip Walls

	$x = 0, 1$	$y = 0, Y$	$z = 0, Z$
ψ_1	$\frac{\partial \psi_1}{\partial x} = \frac{\partial^2 \psi_1}{\partial x^2} = 0$	$\psi_1 = 0, \frac{\partial \psi_1}{\partial y} = \frac{\partial \psi_2}{\partial x} - w$	$\psi_1 = 0, \frac{\partial \psi_1}{\partial z} = \frac{\partial \psi_3}{\partial x} + v$
ψ_2	$\psi_2 = 0, \frac{\partial \psi_2}{\partial x} = \frac{\partial \psi_1}{\partial y} + w$	$\frac{\partial \psi_2}{\partial y} = \frac{\partial^2 \psi_2}{\partial y^2} = 0$	$\psi_2 = 0, \frac{\partial \psi_2}{\partial z} = \frac{\partial \psi_3}{\partial y} - u$
ψ_3	$\psi_3 = 0, \frac{\partial \psi_3}{\partial x} = \frac{\partial \psi_1}{\partial z} - v$	$\psi_3 = 0, \frac{\partial \psi_3}{\partial y} = \frac{\partial \psi_2}{\partial z} + u$	$\frac{\partial \psi_3}{\partial z} = \frac{\partial^2 \psi_3}{\partial z^2} = 0$
ζ_1	$\zeta_1 = 0$	$\zeta_1 = \frac{\partial w}{\partial y} = -\frac{\partial^2 \psi_1}{\partial y^2}$	$\zeta_1 = -\frac{\partial v}{\partial z} = -\frac{\partial^2 \psi_1}{\partial z^2}$
ζ_2	$\zeta_2 = -\frac{\partial w}{\partial x} = -\frac{\partial^2 \psi_2}{\partial x^2}$	$\zeta_2 = 0$	$\zeta_2 = \frac{\partial u}{\partial z} = -\frac{\partial^2 \psi_2}{\partial z^2}$
ζ_3	$\zeta_3 = \frac{\partial v}{\partial x} = -\frac{\partial^2 \psi_3}{\partial x^2}$	$\zeta_3 = -\frac{\partial u}{\partial y} = -\frac{\partial^2 \psi_3}{\partial y^2}$	$\zeta_3 = 0$

5. Transient Convergence and Economy

The characteristics of the method were studied using the natural convection problem described in the previous section. This enabled our results to be compared with those of Rubel and Landis [11], who solved the following equivalent system of equations:

$$\frac{\partial \psi_2}{\partial x} \nabla^2 \left(\frac{\partial \psi_2}{\partial z}\right) - \frac{\partial \psi_2}{\partial z} \nabla^2 \left(\frac{\partial \psi_2}{\partial x}\right) = -\mathrm{RaPr} \frac{\partial \theta}{\partial x} + \mathrm{Pr}\, \nabla^2 \psi_2, \tag{28}$$

$$\frac{\partial \psi_2}{\partial x} \frac{\partial \theta}{\partial z} - \frac{\partial \psi_2}{\partial z} \frac{\partial \theta}{\partial x} = \nabla^2 \theta. \tag{29}$$

TABLE II

Summary of Two-Dimensional Solutions for the "Window" Problem Solved Using a 21 by 51 Mesh (Assuming Antisymmetry) on a CDC 6600 Computer

Run no.	Ra	Pr	α_ζ	$\Delta t/\Delta x^2$	Number of iterations	Solution time (sec)	Starting conditions
1	60,000	1	0.025	6	211	29.4	Rest
2	120,000	1	0.025	6	243	33.7	Run 1
3	180,000	1	0.01	10	262	36.3	Run 2
4	240,000	1	0.01	10	373	51.8	Run 3
5	120,000	2000	0.025	4	291	40.6	Rest
6	180,000	2000	0.025	4	214	29.9	Run 5
7	240,000	2000	0.025	4	215	30.0	Run 6
8	300,000	2000	0.025	4	196	27.4	Run 7
9	180,000	6	0.025	4	209	29.0	Rest
10	300,000	6	0.025	4	216	30.1	Run 9
11	360,000	6	0.025	4	206	28.7	Run 10
					Total solution time = 366.9		

They used a generalized Newton's method to solve the fourth-order nonlinear difference approximation to (28) coupled to a relaxation procedure in a combined inner and outer iteration scheme. Calculations were performed on a CDC 6600 computer, and advantage was taken of the symmetry of the problem to halve the solution domain. For an aspect ratio of five, solutions were obtained for the

inner iterations for each outer iteration; from 25 to 200 outer iterations were required for each solution. The total production time for the 11 cases in Table II was 2.5 hr.

Initially, calculations were performed using $\alpha_\psi = \alpha_\zeta = 1$, but at high Ra and low Pr the solution fields oscillated, the rate of decay being very slow. Adjustment of the transient had a pronounced effect on these oscillations. Reducing α_ψ increased the rate of decay of the oscillations but decreased their frequency, causing slow rates of change of the solution fields. This resulted in either premature termination of the iterations or excessive computation times. Reasoning that the oscillations were driven by the source term in the vorticity equation (as implied by the discussion in the final paragraph of Section 3.2), α_ζ was reduced. This

damped the oscillations and their frequency was now relatively unaffected. As α_ξ was reduced, the time step could be increased, as shown in Table II, and the total solution time was lowered considerably. It can be seen that the effective values of $\Delta t/\Delta x^2$ were 0.1–0.15 for the vorticity equation and 4–10 for the stream function and energy equation. In other words, the effective time step for the latter equations was increased above the empirical limit of $0.8\,\Delta x^2$ by the same factor as it was reduced for the vorticity equation. It should be pointed out that such oscillations can be reduced only if a steady solution exists as was known to be the case for this problem.

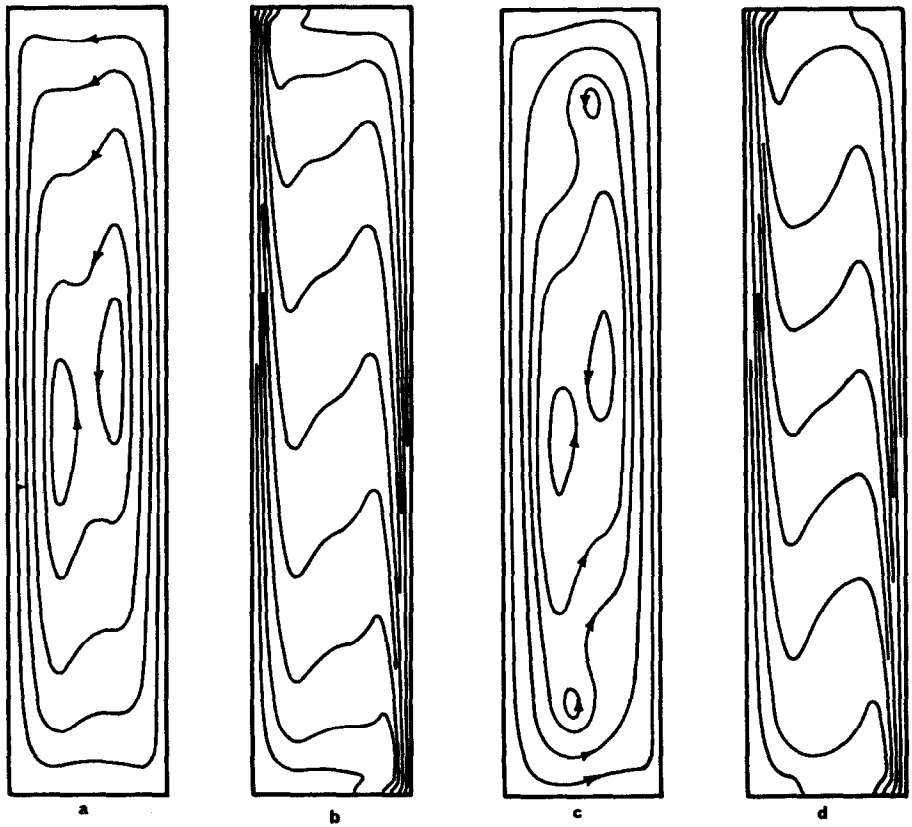

FIG. 2. Two-dimensional solutions for the "window" problem. Aspect ratio = 5. (a), (b) Contours of stream function and temperature for the case Ra = 300,000 and Pr = 6. Contour levels for ψ_2 are 10, 25, 36, 44, and 47. Contour levels for θ are 0.1(0.1)0.9. (c), (d) Contours for the case Ra = 180,000 and Pr = 1. Contour levels for ψ_2 are 5, 20, 30, 32, 34, and 38. Contours for θ as in (b).

Typical solutions are shown in Fig. 2. It was found that the oscillations were associated with the appearance of the small cells which can be seen in Fig. 2c near the top and bottom of the cavity, and which develop at high values of the Grashof number Gr = Ra/Pr. It seems that this problem was a particularly severe test of the method, since natural convection problems with other thermal boundary conditions have been readily solved at even higher parameter values with a minimum of adjustment of α_ζ .

To evaluate the economy of the method, the eleven cases solved by Rubel and Landis were also run on a CDC 6600. The results are summarized in Table II. The average time for each iteration was 0.15 sec, and the total production time was 0.102 hr. Symmetry was assumed and convergence criteria equivalent to those of Rubel and Landis were used; the fact that convergence was reached was verified by decreasing the convergence criterion by an order of magnitude and observing that the solution changed only in the fifth significant figure relative to the function maxima. A similar effect was reported by Rubel and Landis. Based on these results it appears that at the time the tests were performed this method was 25 times as fast as that used by Rubel and Landis. Conservatively, therefore, we suggest an order of magnitude increase in speed has been obtained. However, a number of improvements to the coding have been made since then. Tests on our computer indicate that a further factor of at least two has been achieved.

The reduced computing time required by this method is attributed to the use of a single, rather than a double iterative scheme, and to the stability of the A.D.I. procedure, which enables the false transient to be selected in a manner which enhances the rate of transient convergence.

6. Application to a Three-Dimensional Problem

The problem described in Section 5 has been the subject of numerous analytical and numerical investigations (e.g., [6, 7, 10, 11, 24–31]). In all of these, it has been assumed that the motion is adequately described by a two-dimensional model in which variations in the y-direction of Fig. 1 are neglected. Even experimental studies (of which Brooks and Probert [23] provide a recent summary) generally imply that the motion is expected to be two-dimensional by their use of an interferometer to explore the temperature distribution. It is of interest, therefore, to obtain a three-dimensional solution in order to test this assumption.

The basis for the belief that the flow is two-dimensional is that the cavity is "long" in the y-direction and that the boundary conditions are uniform. It has, of course, been recognized that the end walls would have some effect, but it has been hoped that such effects would be confined to short regions near the walls, and that over most of the cavity they could be ignored. Solutions have, therefore,

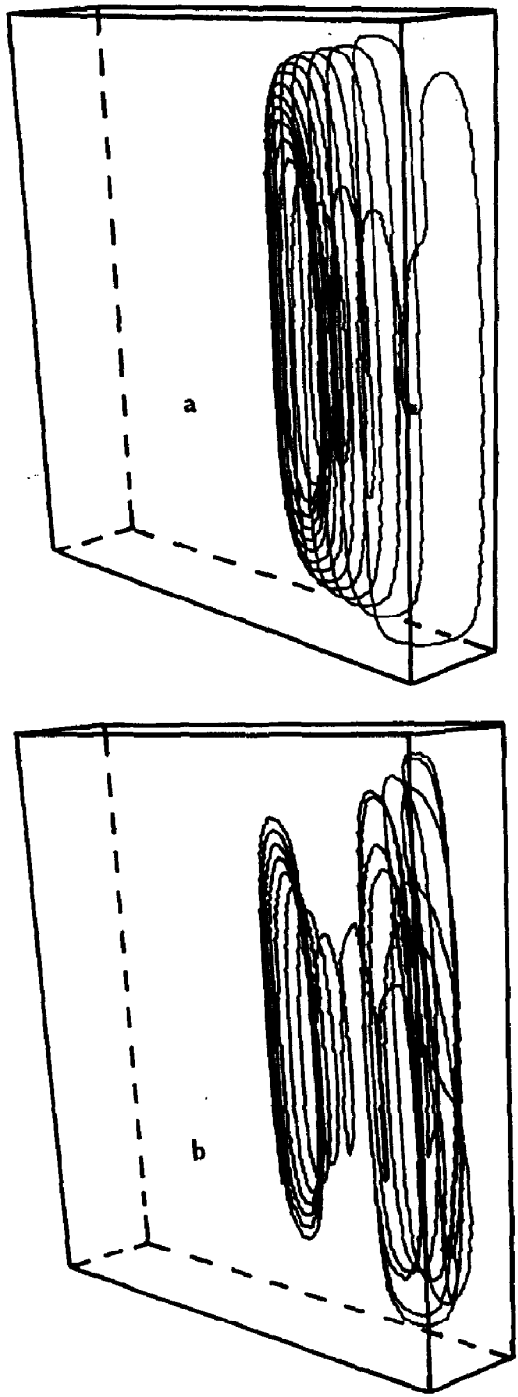

FIG. 3. Particle tracks for a three-dimensional solution of the "window" problem for the case Ra = 10,000, Pr = 1, $Y = 5$, $Z = 5$, solved using an 11 by 21 by 21 mesh. (a) Particle released at (0.5, 4.5, 3.0). (b) Particle released at (0.7, 4.25, 0.5).

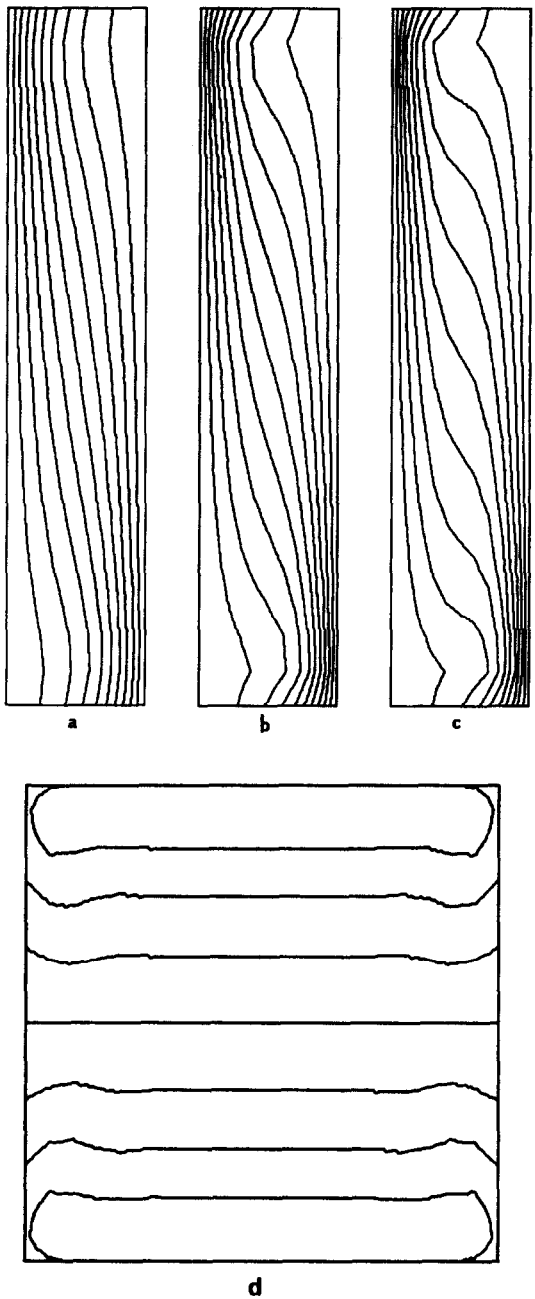

FIG. 4. Temperature contours for the problem of Fig. 3 at various cross-sections. Levels as in Fig. 2. (a) $y = 0$; (b) $y = 0.25$; (c) $y = 2.5$; (d) $x = 0.5$.

been obtained for a cavity in which $Y = 5$ and $Z = 5$. This is a shape which is typical of many of the experimental studies.

The description of a three-dimensional motion in a two-dimensional journal is not easy. We have obtained contour plots of all the computed quantities at a number of horizontal and vertical cross-sections of the cavity, but these do not permit a visualization to be readily obtained. Fig. 3 shows the tracks of two particles released near the end wall $y = 5$. Although such a display is less quantitative than

The particle of Fig. 3(a) was released at the point (0.5, 4.5, 3.0). It moves towards the center of the cavity in a fairly narrow spiral. The horizontal motion ceases near the center plane, and the spiral grows in size. When the particle track approaches the walls of the cavity, a longitudinal motion in the reverse direction is acquired which carries the particle back towards the wall $y = 5$. There, an inward spiral returns the particle to the vicinity of its starting point. It might be expected that the particle should return precisely to its starting point, but as discussed by Truesdell [13], p. 17, there is no a priori reason why the vector lines of a solenoidal field should be closed.

Figure 3(b) shows the track of a particle which was released further from the horizontal axis of the cavity, at the point (0.7, 4.25, 0.5). The motion is more complex, and even harder to visualize. The particle performs three cycles of the type displayed in Fig. 3(a) before it approaches the center plane.

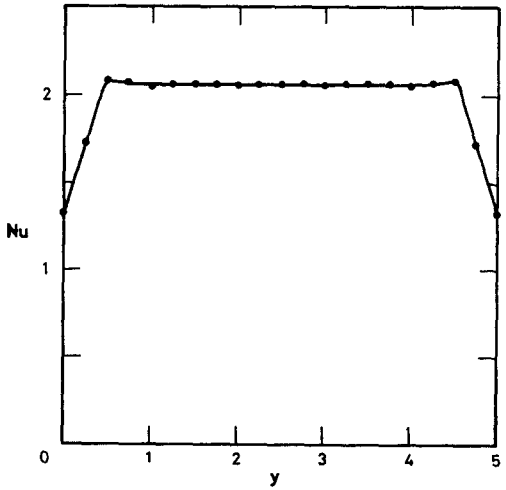

FIG. 5. Variation of vertically averaged Nusselt number across the window for the case of Fig. 3, showing that the thermal effects of the three-dimensional motion are confined to regions of size less than one cavity thickness near each end wall.

The principal conclusion to be drawn is that three-dimensional flow exists throughout the entire cavity. Only when a particle is released on the center plane does it fail to acquire a y-component of velocity. It is now of interest to examine the effects of this motion on the temperature fields.

Figure 4 shows contour maps of the temperature on the planes $y = 0$, 0.25, and 2.5 and $x = 0.5$. It can be seen that within a region of the order of one cavity width from the end walls, the temperature pattern approaches that due to conduction alone. This is clearly a consequence of the viscous effects near these walls which reduce the velocities in the $x - z$ plane and thereby reduce the convective distortion of the temperature field. The y-components of velocity are also due to these effects, but do not appear to have a direct effect on the temperature field because the fluid still follows the basic cellular pattern observed in two-dimensional studies. A quantitative measure of the effect of the end walls can be seen in Fig. 4(d) and also in the variation of the vertically averaged Nusselt number over the plane $x = 0$, shown in Fig. 5. This parameter, which is of practical importance, is related to the normal temperature gradient at the surface. It can be seen that, near the end walls, there is a significant decrease in Nu, but it was found that the overall average value was only 5.5 % less than the value at $y = Y/2$.

Many of the earlier two-dimensional studies considered a cavity of square cross-section. A solution was, therefore, obtained for a cavity in which $Z = 1$, and we chose to set Y at 2. Particle tracks for this situation are shown in Fig. 6. A plan and end elevation have been included. The motion is generally similar to that described previously. It will be noted from the end elevation, however, that the longitudinal spirals are no longer on the central axis of the cavity. There are, in fact, two such spirals in each end of the box, and the double cellular motion observed in two-dimensional solutions at the higher values of Gr is seen to be a contraction of a much more complex flow.

It appears from these limited results that the heat transfer rates are reasonably well predicted by two-dimensional solutions. However, the motion is highly complex and it is clear that a full three-dimensional study is necessary in order that it be properly understood.

Mention should be made of the results of Aziz and Hellums [3], who studied natural convection in a cubical container which was heated from below, cooled from above, and had adiabatic side walls. They examined a range of Rayleigh numbers, the maximum of which was only 3500. Recently, Catton [33] calculated a lower bound of 3446 for the critical Rayleigh number with these boundary conditions. The strength of the motion computed by Aziz and Hellums is, therefore, somewhat surprising. Moreover, they obtained a Nusselt number of 1.88 using an 11 by 11 by 11 mesh. They found that refining the mesh in two dimensions led to a significant decrease in Nu, and this would also be expected in three dimensions. Nevertheless, their result is still in conflict with the experimental work

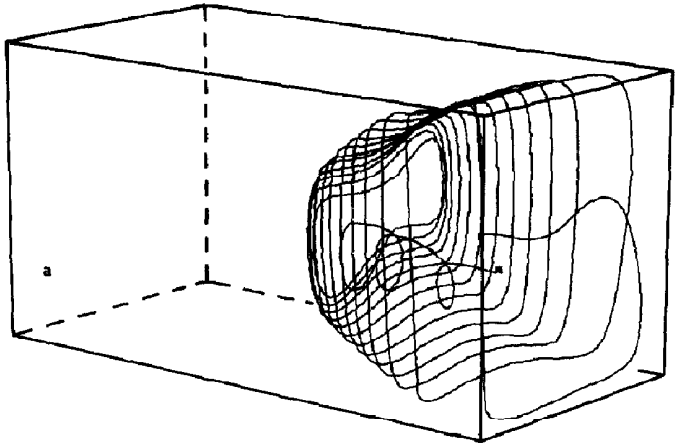
a

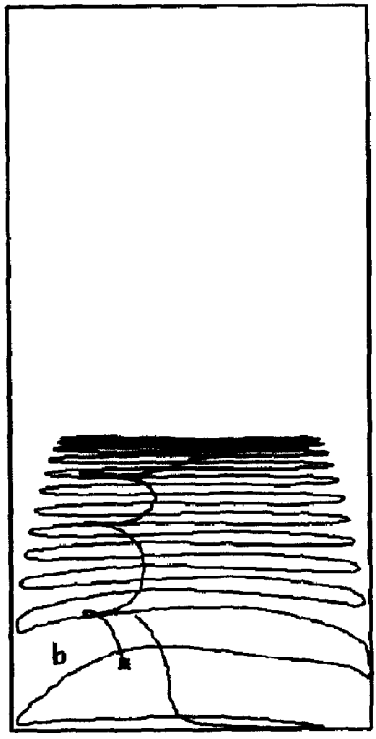
b

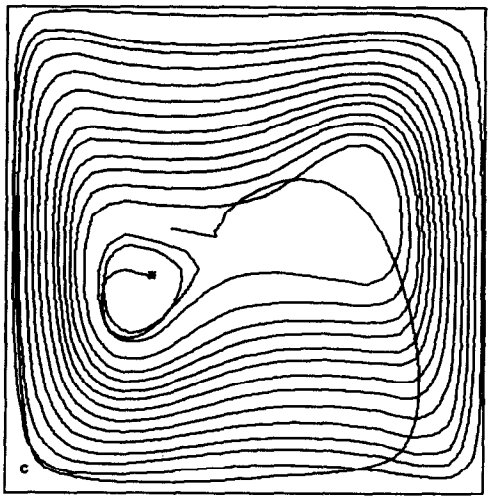

FIG. 6. Particle tracks for the case Ra = 150,000, Pr = 1, $y = 2$, $Z = 1$, solved using a 15 by 15 by 15 mesh. Particle released at (0.3, 1.87, 0.558). (a) Perspective view; (b) plan; (c) end elevation.

of Catton and Edwards [34]. (Although this was performed using a cavity of hexagonal plan-form, the results can be expected to be indicative of those for a cube since the hydraulic diameter of the hexagon was approximately equal to its height.) The critical Rayleigh number was found by them to be about 3500 (in good agreement with Catton's later analysis), and at Ra = 10000, Nu was found to be about 1.78. We found that for Pr = 1.0 the fluid was stable to any disturbance at Ra = 3500 and motion persisted at Ra = 3600; at Ra = 7000, Nu = 1.58; and at Ra = 10000, Nu = 1.80.

We have not made an exhaustive study of the stability of a layer of fluid heated from below. However, it is evident that there are substantial differences between the results of Aziz and Hellums, on the one hand, and those of Catton, Edwards, Mallinson and de Vahl Davis, on the other. We cannot explain these differences.

APPENDIX A: THE COMPONENT EQUATIONS

A.1. *The Differential Equations*

Equations (7), (13)–(15) may be expressed as ten partial differential equations for the ten dependent variables, ζ_1, ζ_2, ζ_3, ψ_1, ψ_2, ψ_3, θ, u, v and w. For rectangular Cartesian coordinates and for $\hat{g} = k$, these may be written

$$\frac{\mathrm{Pr}}{\alpha_\zeta}\frac{\partial\zeta_1}{\partial t} = -\frac{\partial}{\partial y}(\zeta_1 v) - \frac{\partial}{\partial z}(\zeta_1 w) + \frac{\partial}{\partial y}(\zeta_2 u) + \frac{\partial}{\partial z}(\zeta_3 u) - \mathrm{RaPr}\frac{\partial\theta}{\partial y} + \mathrm{Pr}\left(\frac{\partial^2\zeta_1}{\partial x^2} + \frac{\partial^2\zeta_1}{\partial y^2} + \frac{\partial^2\zeta_1}{\partial z^2}\right),$$

$$\frac{\mathrm{Pr}}{\alpha_\zeta}\frac{\partial\zeta_2}{\partial t} = -\frac{\partial}{\partial x}(\zeta_2 u) - \frac{\partial}{\partial z}(\zeta_2 w) + \frac{\partial}{\partial x}(\zeta_1 v) + \frac{\partial}{\partial z}(\zeta_3 w) + \mathrm{RaPr}\frac{\partial\theta}{\partial x} + \mathrm{Pr}\left(\frac{\partial^2\zeta_2}{\partial x^2} + \frac{\partial^2\zeta_2}{\partial y^2} + \frac{\partial^2\zeta_2}{\partial z^2}\right),$$

$$\frac{\mathrm{Pr}}{\alpha_\zeta}\frac{\partial\zeta_3}{\partial t} = -\frac{\partial}{\partial x}(\zeta_3 u) - \frac{\partial}{\partial y}(\zeta_3 v) + \frac{\partial}{\partial x}(\zeta_1 w) + \frac{\partial}{\partial y}(\zeta_2 w) + \mathrm{Pr}\left(\frac{\partial^2\zeta_3}{\partial x^2} + \frac{\partial^2\zeta_3}{\partial y^2} + \frac{\partial^2\zeta_3}{\partial z^2}\right),$$

$$\frac{1}{\alpha_\psi}\frac{\partial\psi_1}{\partial t} = \frac{\partial^2\psi_1}{\partial x^2} + \frac{\partial^2\psi_1}{\partial y^2} + \frac{\partial^2\psi_1}{\partial z^2} + \zeta_1,$$

$$\frac{1}{\alpha_\psi}\frac{\partial\psi_2}{\partial t} = \frac{\partial^2\psi_2}{\partial x^2} + \frac{\partial^2\psi_2}{\partial y^2} + \frac{\partial^2\psi_2}{\partial z^2} + \zeta_2,$$

$$\frac{1}{\alpha_\psi}\frac{\partial\psi_3}{\partial t} = \frac{\partial^2\psi_3}{\partial x^2} + \frac{\partial^2\psi_3}{\partial y^2} + \frac{\partial^2\psi_3}{\partial z^2} + \zeta_3,$$

$$\frac{\partial\theta}{\partial t} = -\frac{\partial}{\partial x}(u\theta) - \frac{\partial}{\partial y}(v\theta) - \frac{\partial}{\partial z}(w\theta) + \frac{\partial^2\theta}{\partial x^2} + \frac{\partial^2\theta}{\partial y^2} + \frac{\partial^2\theta}{\partial z^2},$$

$$u = \frac{\partial\psi_3}{\partial y} - \frac{\partial\psi_2}{\partial z},$$

$$v = \frac{\partial\psi_1}{\partial z} - \frac{\partial\psi_3}{\partial x},$$

$$w = \frac{\partial\psi_2}{\partial x} - \frac{\partial\psi_1}{\partial y}.$$

A.2. *The Finite Difference Approximations*

Using the compact notation defined in Section 3.1, together with

$$\nabla(\zeta_1) = (\zeta_1(i+1) - 2\zeta_1 + \zeta_1(i-1))/\Delta x^2 + (\zeta_1(j+1) - 2\zeta_1 + \zeta_1(j-1))/\Delta y^2 + (\zeta_1(k+1) - 2\zeta_1 + \zeta_1(k-1))/\Delta z^2,$$

the finite difference approximations to the equations of Section A.1 are

$$\begin{aligned}\frac{\mathrm{Pr}}{\alpha_\zeta}\frac{\partial\zeta_1}{\partial t} = &-(v(j+1)\,\zeta_1(j+1) - v(j-1)\,\zeta_1(j-1))/2\,\Delta y\\ &-(w(k+1)\,\zeta_1(k+1) - w(k-1)\,\zeta_1(k-1))/2\,\Delta z\\ &+(u(j+1)\,\zeta_2(j+1) - u(j-1)\,\zeta_2(j-1))/2\,\Delta y\\ &+(u(k+1)\,\zeta_3(k+1) - u(k-1)\,\zeta_3(k-1))/2\,\Delta z\\ &-\mathrm{RaPr}(\theta(j+1) - \theta(j-1))/2\,\Delta y + \mathrm{Pr}\nabla(\zeta_1),\end{aligned}$$

$$\begin{aligned}\frac{\mathrm{Pr}}{\alpha_\zeta}\frac{\partial\zeta_2}{\partial t} = &-(u(i+1)\,\zeta_2(i+1) - u(i-1)\,\zeta_2(i-1))/2\,\Delta x\\ &-(w(k+1)\,\zeta_2(k+1) - w(k-1)\,\zeta_2(k-1))/2\,\Delta z\\ &+(v(i+1)\,\zeta_1(i+1) - v(i-1)\,\zeta_1(i-1))/2\,\Delta x\\ &+(v(k+1)\zeta_3(k+1) - v(k-1)\,\zeta_3(k-1))/2\,\Delta z\\ &+\mathrm{RaPr}(\theta(i+1) - \theta(i-1))/2\,\Delta x + \mathrm{Pr}\,\nabla(\zeta_2),\end{aligned}$$

$$\begin{aligned}\frac{\mathrm{Pr}}{\alpha_\zeta}\frac{\partial\zeta_3}{\partial t} = &-(u(i+1)\,\zeta_3(i+1) - u(i-1)\,\zeta_3(i-1))/2\,\Delta x\\ &-(v(j+1)\,\zeta_3(j+1) - v(j-1)\,\zeta_3(j-1))/2\,\Delta y\\ &+(w(i+1)\,\zeta_1(i+1) - w(i-1)\zeta_1(i-1))/2\,\Delta x\\ &+(w(j+1)\,\zeta_2(j+1) - w(j-1)\,\zeta_2(j-1))/2\,\Delta y\\ &+\mathrm{Pr}\,\nabla(\zeta_3),\end{aligned}$$

$$\frac{1}{\alpha_\psi}\frac{\partial\psi_1}{\partial t} = \nabla(\psi_1) + \zeta_1\,,$$

$$\frac{1}{\alpha_\psi}\frac{\partial\psi_2}{\partial t} = \nabla(\psi_2) + \zeta_2\,,$$

$$\frac{1}{\alpha_\psi}\frac{\partial\psi_3}{\partial t} = \nabla(\psi_3) + \zeta_3\,,$$

$$\begin{aligned}\frac{\partial\theta}{\partial t} = &-(u(i+1)\,\theta(i+1) - u(i-1)\,\theta(i-1))/2\,\Delta x\\ &-(v(j+1)\,\theta(j+1) - v(j-1)\,\theta(j-1))/2\,\Delta y\\ &-(w(k+1)\,\theta(k+1) - w(k-1)\,\theta(k-1))/2\,\Delta z + \nabla(\theta),\end{aligned}$$

$$u = (\psi_3(j+1) - \psi_3(j-1))/2\,\Delta y - (\psi_2(k+1) - \psi_2(k-1))/2\,\Delta z,$$
$$v = (\psi_1(k+1) - \psi_1(k-1))/2\,\Delta z - (\psi_3(i-1) - \psi_3(i-1))/2\,\Delta x,$$
$$w = (\psi_2(i+1) - \psi_2(i-1))/2\,\Delta x - (\psi_1(j+1) - \psi_1(j-1))/2\,\Delta y.$$

APPENDIX B: PARTICLE TRACKING

In steady flow, the particle paths are given by the equations

$$dx/u = dy/v = dz/w.$$

(The paths could also be found from the intersection of the surfaces (9) and (10). However, the calculation of f and g from Ψ is quite complex and the procedure adopted is more straightforward.)

Using $\bar{u} = d\bar{x}/dt$, these equations are integrated numerically by the modified Euler method, which is simple and adequate for the purpose. Denoting the nth point along a particle path by $\bar{x}_n$, and the mth estimate of $\bar{x}_n$ by $\bar{x}_n^m$, the integration algorithm is

$$\bar{x}_{n+1}^1 - \bar{x}_n = \Delta t(\bar{u}(\bar{x}_n)),$$
$$\bar{x}_{n+1}^{m+1} - \bar{x}_n = \Delta t(\bar{u}(\bar{x}_n) + \bar{u}(\bar{x}_n^m))/2, \qquad m = 1, 2, \ldots, k,$$

where k is such that the difference between successive estimates of the new position is less than a specified small quantity, typically 10^{-5}. To limit the particle movement during one integration step, the time interval is chosen to satisfy

$$\Delta t = 0.1\Delta x/\max(|u|, |v|, |w|).$$

These criteria were found, after some experimentation, to yield satisfactory results for a given vector potential field.

It is necessary to construct the velocity field from the vector potential field. The obvious approach is to calculate the velocities at the mesh points and then to interpolate. However, the resultant velocities do not then satisfy continuity and unsatisfactory results are obtained (as was verified during tests on a two-dimensional solution for which the stream lines can be readily obtained).

Accordingly, the components of the vector potential were calculated from

$$\psi_i = a_i + b_i x + c_i y + d_i z + e_i yz + f_i zx + g_i xy + h_i xyz, \qquad i = 1, 2, 3,$$

where the coefficients a_i, b_i, etc. are given in an obvious manner by the mesh point values of ψ_i. The velocity components are then obtained by differentiation. It can be seen that they satisfy continuity.

A further improvement, which has been found to yield smoother tracks, is the construction of a refined Ψ field using interpolation. Typically, an 11 by 11 by 11 mesh would be expanded to 31 by 31 by 31 before entering the tracking procedure. It may be of interest to note that the generation of the track shown in Fig. 3(a) required about 40 sec of CPU time on the 360/50.

It should also be pointed out that Figs. 3 and 6(a) are perspective views, using the transformation given in [35].

ACKNOWLEDGMENTS

G. D. Mallinson is grateful to the Australian Commonwealth Public Service Board for making it possible for him to take part in this research. A grant to G. de Vahl Davis from the Australian Research Grants Committee is also gratefully acknowledged.

REFERENCES

1. G. P. WILLIAMS, *J. Fluid Mech.* **37** (1969), 727.
2. A. J. CHORIN, *Math. Comp.* **22** (1968), 745.
3. K. AZIZ AND J. D. HELLUMS, *Phys. Fluids* **10** (1967), 314.
4. P. H. HOLST AND K. AZIZ, *Int. J. Heat Mass Transfer* **15** (1972), 73.
5. K. TORRANCE, *J. Res. Nat. Bur. Standards Sect. B* **4** (1968), 281.
6. J. O. WILKES AND S. W. CHURCHILL, *AIChE J.* **12** (1966), 161.
7. G. DE VAHL DAVIS, *Int. J. Heat Mass Transfer* **11** (1968), 1675.
8. S. A. PIACSEK AND G. P. WILLIAMS, *J. Comp. Phys.* **6** (1970), 392.
9. C. E. PEARSON, *J. Fluid Mech.* **21** (1965), 611.
10. R. W. THOMAS AND G. DE VAHL DAVIS, Heat Transfer 1970, Vol. 4, Paper NC2.4, Elsevier, Amsterdam, 1971.
11. A. RUBEL AND F. LANDIS, *Phys. Fluids* **12** (1969), 208.
12. J. BOUSSINESQ, "Theorie Analytique de la Chaleur," Vol. 2, p. 172, Gauthier-Villars, Paris, 1903.
13. C. TRUESDELL, "The Kinematics of Vorticity," Indiana Univ. Press, Bloomington, IN, 1954.
14. A. A. DORODNICYN, "Proceedings of the Fourth Australian Computer Conference,"Vol. 2, The Griffin Press, Netley, South Australia, 1969.
15. A. J. CHORIN, *J. Comp. Phys.* **2** (1967), 12.
16. G. J. HIRASAKI AND J. D. HELLUMS, *Quart. Appl. Math.* **16** (1968), 331.
17. A. D. GOSMAN, W. M. PUN, A. K. RUNCHAL, D. B. SPALDING, AND M. WOLFSHTEIN, "Heat and Mass Transfer in Recirculating Flows," Academic Press, London, 1969.
18. A. A. SAMARSKII AND V. B. ANDREEV, *U.S.S.R. Comput. Math. and Math. Phys.* **3** (1963), 1373.
19. J. DOUGLAS, JR., *Numer. Math.* **4** (1962), 41.
20. P. L. T. BRIAN, *AIChE J.* **7** (1961), 367.
21. A. A. SAMARSKII, *U.S.S.R. Comput. Math. and Math. Phys.* **2** (1963), 894.
22. D. W. PEACEMAN AND H. H. RACHFORD, *SIAM J.* **3** (1955), 28.
23. G. DE VAHL DAVIS AND G. D. MALLINSON, University of New South Wales, School of Mechanical and Industrial Engineering, Report 1972/FMT/2, 1972.
24. G. K. BATCHELOR, *Quart. Appl. Math.* **12** (1954), 209.

25. G. DE VAHL DAVIS AND C. F. KETTLEBOROUGH, *Trans. Inst. Eng. Aust.* **MC1** (1965), 43.
26. G. DE VAHL DAVIS AND R. W. THOMAS, *Phys. Fluids* **12** (1969), 198.
27. J. W. ELDER, *J. Fluid Mech.* **23** (1965), 77.
28. A. E. GILL, *J. Fluid Mech.* **26** (1966), 515.
29. R. K. MACGREGOR AND A. F. EMERY, *J. Heat Trans. Ser. C* **91** (1969), 391.
30. M. E. NEWELL AND F. W. SCHMIDT, *J. Heat Trans. Ser. C* **92** (1970), 159.
31. G. POOTS, *Quart. J. Appl. Math.* **11** (1958), 257.
32. R. G. BROOKS AND S. D. PROBERT, *J. Mech. Eng. Sci.* **14** (1972), 107.
33. I. CATTON, *Int. J. Heat Mass Transfer* **15** (1972), 665.
34. I. CATTON AND D. K. EDWARDS, *J. Heat Trans. Ser. C* **89** (1967), 295.
35. B. KUBERT, J. SZABO, AND S. GUILIERI, *J. ACM* **15** (1968), 193.